Intervention with citrus flavonoids reverses obesity and improves metabolic syndrome and atherosclerosis in obese $Ldlr^{-/-}$ mice[s]

Amy C. Burke,*,† Brian G. Sutherland,* Dawn E. Telford,*,§ Marisa R. Morrow,* Cynthia G. Sawyez,*,§ Jane Y. Edwards,*,§ Maria Drangova,** and Murray W. Huff[1],*,†,§

Molecular Medicine* and Imaging Research Laboratories,** Robarts Research Institute, Departments of Biochemistry† and Medicine,§ University of Western Ontario, London, Ontario, Canada N6A 5B7

Abstract Obesity and its associated metabolic dysfunction and cardiovascular disease risk represent a leading cause of adult morbidity worldwide. Currently available pharmacological therapies for obesity have had limited success in reversing existing obesity and metabolic dysregulation. Previous prevention studies demonstrated that the citrus flavonoids, naringenin and nobiletin, protect against obesity and metabolic dysfunction in $Ldlr^{-/-}$ mice fed a high-fat cholesterol-containing (HFHC) diet. However, their effects in an intervention model are unknown. In this report, we show that, in $Ldlr^{-/-}$ mice with diet-induced obesity, citrus flavonoid supplementation to a HFHC diet reversed existing obesity and adipocyte size and number through enhanced energy expenditure and increased hepatic fatty acid oxidation. Caloric intake was unaffected and no evidence of white adipose tissue browning was observed. Reversal of adiposity was accompanied by improvements in hyperlipidemia, insulin sensitivity, hepatic steatosis, and a modest reduction in blood monocytes. Together, this resulted in atherosclerotic lesions that were unchanged in size, but characterized by reduced macrophage content, consistent with a more stable plaque phenotype. These studies further suggest potential therapeutic utility of citrus flavonoids, especially in the context of existing obesity, metabolic dysfunction, and cardiovascular disease.—Burke, A. C., B. G. Sutherland, D. E. Telford, M. R. Morrow, C. G. Sawyez, J. Y. Edwards, M. Drangova, and M. W. Huff. Intervention with citrus flavonoids reverses obesity and improves metabolic syndrome and atherosclerosis in obese $Ldlr^{-/-}$ mice. *J. Lipid Res.* 2018. 59: 1714–1728.

Supplementary key words steatohepatitis • beta oxidation • insulin resistance • hypolipidemic drugs • low density lipoprotein receptor-deficient mice

Fat accumulation, as a result of an imbalance between energy input and expenditure, leads to obesity, type 2 diabetes, cardiovascular disease, and hepatic steatosis, which collectively represent one of the leading causes of adult morbidity and mortality worldwide (1–3). This suggests that restoration of functional energy homeostasis is critical for therapeutic intervention. Despite efforts to develop anti-obesity medications that curtail symptoms of metabolic dysfunction, drugs that have reached the market have limited efficacy for obesity ($\sim$5–8%) and many have been withdrawn for negative side effects (3–6). Currently available therapeutics predominantly work by either reducing caloric intake or blocking food absorption (3). Additionally, patients often regain lost weight. The treatment strategy with the most robust and lasting improvements is gastric bypass surgery, which has shown up to $\sim$25% weight loss at 12 years together with a 51% remission rate for type 2 diabetes (7). Presently, gastric bypass surgery as an intervention for obesity and metabolic syndrome is limited to patients with a BMI $\geqslant$35 kg/m^2 (8), excluding patients with moderate obesity, although these patients often present with increased metabolic dysfunction and cardiovascular risk (9, 10). Therefore, there is urgent need for safe and effective medical therapies for obesity and its associated complications, including the metabolic syndrome and cardiovascular disease.

Epidemiological studies show an inverse correlation between flavonoid (a class of plant-derived polyphenols) consumption and the development of type 2 diabetes, metabolic syndrome, and atherosclerosis (11, 12). Previous research in our laboratory identified the citrus-derived flavonoids,

Abbreviations: ABI, Applied Biosystems; AUC, area under the curve; BAT, brown adipose tissue; CE, cholesteryl ester; eWAT, epididymal white adipose tissue; FPLC, fast-protein LC; HFHC, high-fat cholesterol-containing; HOMA-IR, homeostasis model assessment of insulin resistance; iWAT, inguinal white adipose tissue; micro-CT, micro-computed tomography; RER, respiratory exchange ratio; SMC, smooth muscle cell; TC, total cholesterol; TG, triglyceride.

[1] To whom correspondence should be addressed.
    e-mail: mhuff@uwo.ca

[s] The online version of this article (available at http://www.jlr.org) contains a supplement.

naringenin and nobiletin, as novel therapeutics for the prevention of metabolic syndrome and cardiovascular disease (13–17). These flavonoids have anti-inflammatory properties, promote insulin sensitivity, and inhibit apoB100 secretion from cultured hepatocytes (16, 18–20). When extended to a mouse model of obesity, metabolic dysfunction, and atherogenesis, namely the $Ldlr^{-/-}$ mouse fed a high-fat cholesterol-containing (HFHC) diet, prevention studies revealed that supplementation of the HFHC diet with naringenin or nobiletin attenuated weight gain and adiposity, enhanced insulin signaling, lowered plasma lipids, and prevented systemic inflammation and hepatic steatosis, resulting in slowed atherosclerosis progression (13–17). While these studies highlight potential therapeutic utility of the citrus flavonoids, it would be more clinically relevant to assess the efficacy of these compounds in an intervention protocol where obesity, insulin resistance, hyperlipidemia, and atherosclerosis have been established prior to treatment.

In the present study, we show, in $Ldlr^{-/-}$ mice with pre-established diet-induced obesity, metabolic dysregulation, and intermediate-stage atherosclerosis, that intervention by the addition of either naringenin or nobiletin to a HFHC diet not only prevented continued obesity and deterioration in symptoms of the metabolic syndrome but also markedly reduced adipose tissue mass, normalized glucose homeostasis, and attenuated both hyperlipidemia and hepatic steatosis. Correction of metabolic parameters was accompanied by a reduction in circulating blood monocytes. Collectively, these metabolic improvements did not resolve the size of aortic sinus atherosclerotic lesions, but plaques in flavonoid-treated mice were characterized by reduced macrophage and cholesterol content, consistent with lesion regression (21, 22).

MATERIALS AND METHODS

Animals and diets

Male $Ldlr^{-/-}$ mice on a C57BL/6 background (Jackson Laboratory, Bar Harbor, ME) were housed in pairs in standard cages at 23°C on a 12 h light and dark cycle. The animals were cared for in accordance with the Canadian Guide for the Care and Use of Laboratory Animals. All experimental procedures were approved by the Animal Care Committee at the University of Western Ontario (protocol #AUP-2016-057). Mice, 10–12 weeks of age (n = 10), were fed, ad libitum, a purified rodent chow diet (14% of calories from fat, Teklad Rodent Diet 8604; Envigo, Madison, WI) for 24 weeks. Another group of mice (10–12 weeks of age, n = 120, 24 per group) were fed a HFHC diet (42% of calories from fat, 0.2% cholesterol, Teklad TD09268; Envigo) for 12 weeks (baseline). A subgroup of these HFHC-fed mice (n = 24) were euthanized at 12 weeks to provide baseline data for analyses that required euthanization. The remaining mice were divided among four different groups and, for the subsequent 12 weeks, one group remained on the same HFHC diet (n = 24), one group remained on the HFHC diet supplemented with 3% naringenin (#N5893; Millipore-Sigma) (n = 24), one group remained on the HFHC diet supplemented with 0.3% nobiletin (#10236-47-2; R&S PharmChem, Hangzhou City, China) (n = 24), and one group was switched to the standard rodent chow (n = 24). Food intake and body weights were measured weekly. Caloric intake was calculated as weight of food eaten (grams) per day multiplied by the caloric content of each diet (chow 3.0 kcal/g; HFHC 4.5 kcal/g). We previously observed a taste aversion with naringenin and nobiletin, which was mitigated by slowly increasing the flavonoid dose over the first week of intervention to prevent significant impact on food intake (data not shown).

Blood and tissue collection

Mice were fasted for 6 h at the start of the light cycle prior to blood taking or euthanization. At the time of euthanization, animals were anesthetized with ketamine-xylazine [100 µg/g ketamine hydrochloride (Bioniche Animal Health Canada Inc., Belleville, ON, Canada) and 10 µg/g xylazine (Bayer Healthcare, Animal Health Division, Bayer Inc., Toronto, ON, Canada)]. Blood was collected via cardiac puncture in syringes containing 80 µl of 7% Na_2-EDTA. Blood was centrifuged at 16,000 g for 10 min at 4°C to separate the plasma, which was stored at −20°C for further use. Tissue dissections were performed via midline incision. To dissect the heart for histological analysis, the left ventricle was perfused with PBS containing heparin (10 units/ml) and the right atrium was cut to drain the perfusate. The heart and full-length aorta were dissected together. Aortae were rinsed and cleaned using a dissecting microscope to remove any adipose tissue. Aortae were snap-frozen in liquid N_2 and stored at −80°C for mRNA and lipid measurements. The top half of the heart was placed in OCT medium, frozen on dry ice, and stored at −80°C for histological analyses. Small pieces of both epididymal and inguinal white adipose tissue (eWAT, iWAT) were fixed in 4% paraformaldehyde and paraffin embedded for histological analyses. Liver, eWAT, iWAT, brown adipose tissue (BAT), and quadricep, gastrocnemius, and soleus muscles were removed, weighed, and snap-frozen in liquid N_2 and stored at −80°C.

Metabolic cages

From 1 to 4 weeks prior to completion of the intervention period, energy expenditure, respiratory exchange ratio (RER), food consumption, and locomotor activity were assessed using the Comprehensive Laboratory Animal Monitoring System (CLAMS; Columbus Instruments, Columbus, OH). Mice were housed in metabolic cages with free access to food and water and acclimatized for 48 h. For the subsequent 24 h, every 10 min, data on O_2 consumption (VO$_2$; milliliters per hour) and CO_2 production (VCO$_2$; milliliters per hour) were collected. The RER was derived from the ratio of VCO$_2$ to VO$_2$, and energy expenditure was determined as $(3.815 + 1.232 \times RER) \times VO_2$ and expressed as ANCOVA-adjusted energy expenditure in kilocalories per hour. ANCOVA adjustments to energy expenditure were made based on body weight, which allowed for the determination of differences in energy expenditure independent of group differences in body weight. The ANCOVA analysis performed for this work was provided by the National Institute of Diabetes and Digestive and Kidney Diseases Mouse Metabolic Phenotyping Centers (MMPC; www.mmpc.org) using their Energy Expenditure Analysis page (http://www.mmpc.org/shared/regression.aspx). Ambulatory activity was measured as infrared beam breaks in the X, Y, and Z axis per hour. Accumulated food consumption was measured in grams and converted to kilocalories based on diet composition.

Micro-computed tomography

Mice were first imaged at 12 weeks (baseline) on diet (n = 8 per group) and regularly following intervention (weeks 14, 16, 18, 21, and 23), as described previously (13). Whole-body composition analysis was conducted by micro-computed tomography

(micro-CT) imaging using a Locus Ultra micro-CT scanner (GE Healthcare) (23). Following a 4 h fast, mice were anesthetized with 1.5% isoflurane in O_2. The scan protocol consisted of an X-ray tube voltage of 80 kVP and a current of 55.0 mA. A calibrating phantom, comprising air and water, was scanned concurrently as a calibrator that enabled the conversion of the reconstructed image values into CT numbers [Hounsfield units (HU)]. In a scan time of 16 s, 1,000 views were acquired in one continuous rotation. Images were reconstructed to an isotropic voxel size of 150 μm^3. The analysis was conducted using MicroView software version 2.2 (GE Healthcare). Total adipose tissue volume was calculated by selecting all voxels with values within a window of -225 to -60 HU and then divided into subcutaneous and visceral depots. Subcutaneous and visceral adipose tissue depots were differentiated using the muscular abdominal wall, which is readily identifiable because of its higher density (24). The subcutaneous and visceral adipose depots were outlined manually and the volume of each region was calculated by MicroView as the number of voxels falling within the threshold window multiplied by voxel volume (150 μm^3).

Glucose and insulin tolerance tests

A glucose tolerance test was performed following a 6 h fast by intraperitoneal injection with 15% glucose in 0.9% NaCl (1 g/kg body weight) (15). Blood samples for glucose measurements (Bayer contour blood glucose monitoring system; Bayer Healthcare) were taken up to 120 min postinjection. An insulin tolerance test was conducted following a 5 h fast by intraperitoneal injection with insulin (0.6 IU/kg body weight; Novolin GE Toronto, Novo Nordisk, Cooksville, ON, Canada) (15). Blood samples for glucose measurements were obtained up to 60 min postinjection. Glucose and insulin tolerance were calculated as a percent change in blood glucose from baseline.

Tissue lipids

Lipids from liver, quadriceps, gastrocnemii, and solei, and full-length aortae dissected free of fat and connective tissue were extracted using the method of Folch from samples stored at $-80°C$, as described previously (14, 25). The [cholesteryl-1,2-^{3}H(N)]cholesteryl oleate (PerkinElmer, Guelph, Canada; #NET746L) was added to assess recovery. A combined 200 μg/ml triolein and 200 μg/ml cholesterol standard was prepared in isopropanol and aliquoted for standard curves (0–20 μg). Samples and standards were dried under N_2 and a 1% Triton X-100 solution in chloroform added and left at room temperature for 1 h to solubilize. Samples and standards were dried under N_2, followed by the addition of deionized water and incubation at 37°C for 15 min. Samples were analyzed using enzymatic reagents for triglyceride (TG) (Roche Diagnostics, Laval, Canada; TGs/glycerol blanked, #11877771 216), total cholesterol (TC) (WAKO Diagnostics, Richmond, VA; cholesterol E (CHOD-DAOS method), #439-17501), and free cholesterol (WAKO Diagnostics; free cholesterol (COD-DAOS) method, #435-35801). Cholesteryl ester (CE) was determined as the difference between TC and free cholesterol.

Plasma measurements

Plasma TG and TC were measured on a Cobas Mira S autoanalyzer (Roche Diagnostics) using calibrators and controls from Roche Diagnostics (15). Enzymatic reagents for TG (Roche Diagnostics; TGs/glycerol blanked, #11877771 216) and cholesterol (Roche Diagnostics; Cholesterol CHOD-PAP, #11491458-216) were used. Fresh-EDTA plasma (50 μl) was separated by fast-protein LC (FPLC) using an AKTA purifier and a Superose 6 column (14). A constant flow rate of 0.4 ml/min was used to collect 500 μl fractions. An aliquot of each fraction was used to measure cholesterol

and TGs enzymatically in both samples and standards on a microtiter plate with added enzymatic reagents [TG: Roche Diagnostics, TGs/glycerol blanked, #11877771 216 and TC: WAKO Diagnostics, Cholesterol E: (CHOD-DAOS method), #439-17501]. Blood glucose was measured in whole blood using the Bayer contour blood glucose monitoring system (Bayer Healthcare, Etobicoke, Canada) (15). Plasma insulin (ALPCO Diagnostics, Salem, NH; mouse ultrasensitive ELISA #80-INSMSU-E01) was determined in EDTA-plasma samples, stored at $-80°C$, by a mouse-specific ELISA. Homeostasis model assessment of insulin resistance (HOMA-IR) was calculated using the following formula, as previously described for mice: HOMA-IR = 26 × fasting insulin level (ng/ml) × fasting glucose level (mg/dl)/405 (26).

Liver beta oxidation

For hepatic fatty acid oxidation, fresh liver (250 mg) was homogenized in 0.1 M phosphate buffer (pH 7.2) containing 0.25 M sucrose, 1 mM EDTA, 1 mM dithiothreitol, and 10 μl/ml of protease inhibitor (Sigma-Aldrich; #P8340). Homogenates were centrifuged at 1,000 g at 4°C for 10 min. Twenty microliters of supernatant were incubated for 30 min at 37°C with constant shaking in 0.1 M phosphate buffer (pH 7.2) containing 150 mM KCl, 10 mM HEPES, 5 mM Tris malonate, 10 mM $MgCl_2$, 1 mM carnitine, 5 mM ATP, and 2 μCi of [9,10-^{3}H(N)]palmitic acid (PerkinElmer; #NET043001MC) per 50 μM unlabeled palmitic acid complexed with 0.15% fatty acid-free BSA. Reactions were stopped with 200 μl of 0.6 N perchloric acid and unreacted fatty acids extracted with hexanes. The ^3H_2O in the aqueous phase was measured by liquid scintillation counting (15, 27).

Gene expression

RNA was isolated from aliquots of liver, eWAT, iWAT, BAT, and whole aortae using Trizol reagent (Life Technologies, Mississauga, ON, Canada). Reverse transcription of 1 μg total RNA was performed using a high-capacity reverse transcription kit (Applied Biosystems; ABI) to yield cDNA. Specific mRNA abundances were measured by quantitative real-time PCR on an ABI ViiA 7 sequence detection system according to the manufacturer's instructions. In the eWAT, iWAT, and BAT, mRNA quantitation for *Tnfa*, *Ccl2*, *Ccl3*, *Emr1*, *Ucp1*, *Cidea*, *Pdk4*, *Ppara*, *Lipe*, and *Pnpla2* was determined. In liver, mRNA quantitation for *Cpt1a*, *Pgc1a*, *Srepf1c*, *Ppara*, *Acox1*, *Ccl2*, *Ccl3*, and *Tnfa* was determined. In the aorta, mRNA quantitation for *Ccl3*, *Il1b*, *Ccl2*, *Tnfa*, *Emr1*, *Ccr7*, *Abca1*, and *Abcg1* was determined. Samples (10 ng) of cDNA were assayed in triplicate in 10 μl reactions using a standard curve quantitative real-time PCR protocol to calculate specific mRNA concentrations. Expression levels for each gene were normalized to *Gapdh* expression in each tissue. With the exception of *Srebf1c*, all primer and probe sets used were purchased as TaqMan assays (ABI). The probe and primer sequences for *Srebf1c* were designed from the known murine *Srebf1* locus to determine splice junctions. The intervening intronic sequence was removed and primers and a probe were designed from the resultant *Srebp1c* exon1c-exon2 sequence using Primer Express 2.0 software (ABI). Primers were obtained from Sigma-Genosys and the probes labeled 5′ with 6-carboxyfluorescein (FAM) and 3′ with the quencher, MGB®, were from ABI (TaqMan assay for mouse *Srebf1c*: forward primer, CAGGCCCGGGAAGTCACT; reverse primer, GACCACGGAGCCATGGATT; probe, FAM-ATTTGAAGACATGCTCCA-MGB®).

Tissue histology and immunohistochemistry

Histological and morphometric analyses were performed as described previously (14, 17). eWAT was fixed in 4% paraformaldehyde for 24 h, processed, embedded in paraffin, sectioned on a

Microm HM335E microtome (Thermo Fisher Scientific), and stained with H&E. Frozen serial sections (70–100 per heart, 10 μm) of the aortic sinus from hearts frozen in OCT, initiating anterior to the origin of the aortic valves, were prepared using a Leica CM 3050S cryostat. For quantitation of lesion area in the aortic sinus, sections were stained with oil red-O. Immunohistochemistry staining for macrophages by CD68 (Bio-Rad, Mississauga, Canada; MCA 1957), smooth muscle α-actin (Abcam, Toronto, Canada; polyclonal rabbit anti-smooth muscle α-actin, ab5694), and activated caspase-3 (Abcam; rabbit anti-active caspase-3, ab4051) was performed as described previously (28). Slides were fixed in acetone and blocked in 2% BSA (Sigma-Aldrich). After incubation with primary antibody, a goat biotinylated secondary antibody was used (Vector Laboratories, Burlington, ON, Canada). Slides were then incubated in peroxidase blocking reagent, followed by incubation with the ABC reagent (ABC Elite Standard kit; Vector Laboratories). Slides were exposed to the DAB substrate (peroxidase substrate kit; Vector Laboratories) followed by counterstain in hematoxylin (Sigma-Aldrich). Photomicrographs were obtained using an Olympus BX50 microscope and a QImaging Retiga EXi FAST camera. Collagen fibrils were assessed using circular polarizing microscopy as described previously (28). Aortic sinus sections were stained with picrosirius red (Polysciences, Warrington, PA) and visualized using an Olympus BX51 microscope (Olympus Canada, Richmond Hill, Canada) equipped with circular polarizer/interference filters, a liquid crystal compensator, a charge-coupled device video camera, and Abrio image-processing software (Abrio LC-Polscope; Cambridge Research and Instrumentation, Inc., Hopkinton, MA).

Morphometric analysis of lesion area, necrotic core area, CD68, smooth muscle α-actin, and collagen in lesions from mice from each group was performed on serial sections. The relative area of the atherosclerotic plaque positive for CD68, smooth muscle α-actin, or collagen was determined as the area of positive staining divided by the area of the respective plaque. Quantitation was determined using ImageJ 1.50 software (National Institutes of Health) for CD68, smooth muscle α-actin, and collagen, or AxioVision software for lesion area and necrotic core size. To determine the relative activation of caspase-3, the number of cell nuclei immunostained for activated caspase-3 was expressed as a percentage of the total lesion area. To ensure that a standard region was measured in each mouse, lesion analyses began at the origin of the aortic valves. All quantitations were performed independently by three people.

Flow cytometry

Blood and bone marrow cell analyses were performed in a separate experiment in $Ldlr^{-/-}$ mice (n = 8 per group) using the same induction and intervention protocol described above.

Blood leukocytes. Monocytes and neutrophils were identified from whole blood. At euthanization, blood was collected by cardiac puncture into EDTA-lined tubes and immediately placed on ice. For each mouse sample, 100 μl of blood was used. UltraComp eBeads (Affymetrix eBiosciences, Cedarlane, Burlington, ON, Canada; #01-2222) were used as a single positive control, except for the single positive control for the Vital Dye, where ArC™ amine reactive compensation bead kit was used (A10346; Life Technologies, Burlington, ON, Canada). Fluorescence minus one controls were performed on combined blood samples from all mice, 100 μl each. Viability was assessed using LIVE/DEAD® fixable dead cell near-IR stain kit (L11019; Invitrogen, Life Technologies) (supplemental Table S1) in all samples after incubation for 25 min in the dark at room temperature. Cells were stained with a cocktail of antibodies against CD45-eFluor®450 (Affymetrix eBiosciences, Cedarlane), Ly6-C/G-PerCP-Cy™5.5

(BD Biosciences, Cedarlane, Burlington, ON, Canada), and CD115-APC (Affymetrix eBiosciences) on ice for 20 min in the dark (supplemental Table S1), similar to previous studies (29). Red blood cells were lysed in 1× PharmLyse (BD Biosciences) for 13 min at room temperature. The stained white blood cells were centrifuged, washed, and resuspended in flow-buffer (HBSS + 0.1% BSA, w/v). Cells were fixed by the addition of 4% paraformaldehyde. Monocytes were identified as $CD45^{hi}$ $CD115^{hi}$ and further identified into $Ly6-C^{hi}$ and $Ly6-C^{lo}$; neutrophils were identified as $CD45^{hi}$ $CD115^{lo}$ $Ly6-C/G^{hi}$ (Gr-1), similar to previous studies (supplemental Fig. S1A) (29).

Hematopoietic stem cells. Hematopoietic stem and progenitor cells from the bone marrow were analyzed by flow cytometry. Bone marrow was harvested from femurs and tibias by flushing with HBSS + 0.1% BSA w/v through a 70 μm cell strainer. The cell suspension was centrifuged for 5 min at 500 g at 6°C, supernatant aspirated, and the cells resuspended in 1× PharmLyse (BD Biosciences) for 5 min. Red blood cell lysis was stopped by the addition of excess HBSS + 0.1% BSA. Cells were once again centrifuged at 500 g for 5 min at 6°C and the supernatant aspirated. Cells were resuspended in 1 ml HBSS + 0.1% BSA and blocked with normal goat serum. Cells were once again centrifuged at 500 g for 5 min at 6°C and the supernatant aspirated. Bone marrow was resuspended in 4 ml of HBSS + 0.1% BSA. For each mouse bone marrow sample, 150 μl of suspension were used. UltraComp eBeads (Affymetrix eBiosciences; #01-2222) were used as a single positive control, except for the single positive control for the Vital Dye, where the ArC™ amine reactive compensation bead kit was used (A10346; Life Technologies). Fluorescence minus one controls were done on combined samples from all mice, 150 μl each. Viability was assessed using LIVE/DEAD® fixable dead cell near-IR stain kit (L11019; Invitrogen, Life Technologies) (supplemental Table S1) in all samples after incubation for 25 min in the dark at room temperature. Cells were stained with a cocktail of antibodies against FITC mouse hematopoietic lineage cocktail [CD3 (17A2), CD45R (B220)(RA3-6B2), CD11b (M1/70), TER-119, Ly-G6 (Gr-1) (RB6-8C5)] (Affymetrix eBiosciences), Brilliant Violet 421™ anti-mouse CD117 (c-Kit) (Biolegend, Cedarlane), Brilliant Violet 605™ anti-mouse Ly-6A/E (Sca-1) (Biolegend), Alexa Fluor®700 anti-mouse CD16/32 (Affymetrix eBiosciences), and PE anti-mouse CD34 (Biolegend) on ice for 20 min in the dark (supplemental Table S1) similar to previous studies (29). The stained white blood cells were centrifuged, washed, and resuspended in flow-buffer (HBSS + 0.1% BSA, w/v). Cells were fixed by the addition of 4% paraformaldehyde. Hematopoietic stem and progenitor cells were identified as Lin^-, $Sca-1^+$, and $ckit^+$, while the hematopoietic progenitor subsets were separated using antibodies to CD16/32 (FcγRII/III) and CD34. Common myeloid progenitors were identified as lin^-, $Sca-1^-$, $ckit^+$, $CD34^{hi}$, and $FcγRII/III^{lo}$; granulocyte macrophage progenitors were identified as lin^-, $Sca-1^-$, $ckit^+$, $CD34^{hi}$, and $FcγRII/III^{hi}$; megakaryocyte and erythrocyte progenitors were identified as lin^-, $Sca-1^-$, $ckit^+$, $CD34^{lo}$, and $FcγRII/III^{lo}$ (supplemental Fig. S1B).

Flow cytometry was performed using an LSRII (for analysis) running FACS DiVa software. All flow cytometry data were analyzed using FlowJo software (Tree Star Inc.)

Statistical analysis

Data are presented as mean ± SEM. Statistical analyses were performed using Sigma Plot version 14.0. A one-way ANOVA with post hoc Tukey's test was used to test for differences between groups, except in the case of body weight and adiposity measured over time where a two-way repeated measures ANOVA with post hoc Tukey's test was used. Significance thresholds were $P < 0.05$. Significance differences are indicated by different lowercase letters. A Student's t-test was used to test for differences in

ANCOVA-adjusted energy expenditure. Significant differences ($P < 0.05$) are indicated by an asterisk.

RESULTS

Flavonoid intervention promotes weight loss and attenuates adiposity

Previously, we determined that addition of either naringenin or nobiletin to a HFHC diet prevented the development of many of the disorders of the metabolic syndrome and prevented atherosclerosis (15–17). To determine the therapeutic utility of these flavonoids, we sought to assess their efficacy in an intervention model where these disorders were preestablished. Mice were initially fed a HFHC diet over 12 weeks to induce obesity, metabolic syndrome, and intermediate atherosclerotic lesions, and establish a disease baseline to which the efficacy of intervention was evaluated (**Fig. 1A**). Subsequently, mice were divided among four treatment groups for the subsequent 12 weeks: one group remained on the HFHC diet; a second group received intervention with regular mouse chow; a third group received intervention with the HFHC diet supplemented with 3% naringenin; and the fourth group received intervention with the HFHC diet supplemented with 0.3% nobiletin (Fig. 1A).

All mice gained weight over the initial 12 week induction phase. Subsequently, mice that remained on the HFHC diet increased their body weight a further 20% (Fig. 1B). Mice that received intervention with naringenin or nobiletin, while also remaining on the same HFHC diet, lost ~13% of the body weight gained during the induction phase, a loss similar to that observed in the chow diet intervention group (Fig. 1B). Chow intervention suppressed food intake during the first week, due to the abrupt change in food texture, but was rapidly resolved (Fig. 1C). Intervention with the addition of naringenin or nobiletin to the HFHC diet did not significantly reduce caloric intake throughout the 12 weeks of intervention, suggesting that there was no flavonoid effect on satiety or feeding behavior (Fig. 1C).

Epididymal fat depots were increased during induction with the HFHC diet (Fig. 1D). Compared with baseline, intervention with naringenin or nobiletin reduced epididymal fat by 29% and 44%, respectively, similar to the fat loss in chow-intervened mice (Fig. 1D). By contrast, in mice that remained on the HFHC diet alone, epididymal fat mass increased by 28%. The same trends were observed for inguinal adipose tissue (supplemental Fig. S2A). In a separate study, we confirmed the intervention-induced adipose tissue reductions with the flavonoids by micro-CT (Fig. 1E, supplemental Fig. S2B). Micro-CT showed that visceral fat volume was reduced 38–53% and subcutaneous fat volume was reduced 23–43% by flavonoid intervention (Fig. 1E, supplemental Fig. S2B). Importantly, lean tissue volume did not significantly change during the 12 weeks of intervention (Fig. 1F), indicating that the intervention-induced weight loss was driven by a reduction in adiposity.

Flavonoid intervention reduced adipose tissue inflammation

Previous prevention studies demonstrated that naringenin attenuated adipocyte hypertrophy and adipose tissue inflammation in HFHC-fed $Ldlr^{-/-}$ mice (14). In the present study, compared with mice that remained on the HFHC diet, intervention by either naringenin, nobiletin, or chow induced a shift in epididymal adipocyte area toward smaller adipocytes by 19, 23, and 30%, respectively (Fig. 1G). Similarly, flavonoid-treated mice had smaller adipocytes in inguinal adipose tissue (supplemental Fig. S2A). We next measured the mRNA expression of inflammatory genes in eWAT, iWAT, and BAT. Consistently, intervention with naringenin or nobiletin reduced mean mRNA expressions of *Tnfa*, *Ccl2*, and *Ccl3*, similar to reductions observed with chow intervention. Although not statistically significant, these reductions suggest a shift to resolution of obesity-associated adipose tissue inflammation (supplemental Fig. S3A). To try to understand whether the reduction in adiposity was due to browning or enhanced lipolysis, the mRNA expression of known markers of adipose tissue browning and lipolysis was measured. Treatment with nobiletin, but not naringenin or chow, increased the mean *Ucp1* mRNA expression in epididymal and inguinal adipose tissue (not significant). No intervention altered *Ucp1* expression in BAT (supplemental Fig. S3B). Neither intervention with naringenin, nobiletin, nor chow affected mRNA expression of other browning markers, *Cidea*, *Pdk4*, and *Ppara*, or the lipolysis-associated genes, *Lipe* and *Pnpla2*, in iWAT, eWAT, or BAT (supplemental Fig. S3B, C). This suggests that the reduction in adiposity with each intervention was not likely mediated directly through browning or enhanced lipolysis within white adipose tissue. Histological assessment of BAT revealed that naringenin or nobiletin intervention reduced tissue lipid accumulation similar to intervention with chow (supplemental Fig. S3D).

Flavonoid intervention increases energy expenditure

Previous prevention studies have shown that the addition of either flavonoid to the HFHC diet increased weight-normalized energy expenditure in mice (14, 16). Therefore, we assessed whether flavonoid intervention would also correct obesity-associated suppressed energy expenditure. Following HFHC diet induction, intervention with either naringenin or nobiletin increased ANCOVA-adjusted energy expenditure in both the light and dark cycles, compared with mice that continued on the HFHC diet alone, suggesting a compound-mediated mechanism (**Fig. 2A**). The RER, which is indicative of metabolic fuel source, was also altered by flavonoid intervention. Mice that continued on the HFHC diet alone had a mean RER in the light cycle of 0.82, which decreased to 0.75 in the dark cycle, indicative of fat as the primary metabolic fuel source over 24 h (Fig. 2B). Interestingly, intervention with either flavonoid to the HFHC diet maintained an RER ~0.8 during the dark cycle, when mice consume the majority of their daily caloric intake (30). This indicates a shift to a combination of carbohydrate and fat utilization in the flavonoid-treated mice (Fig. 2B). Intervention with the chow diet increased
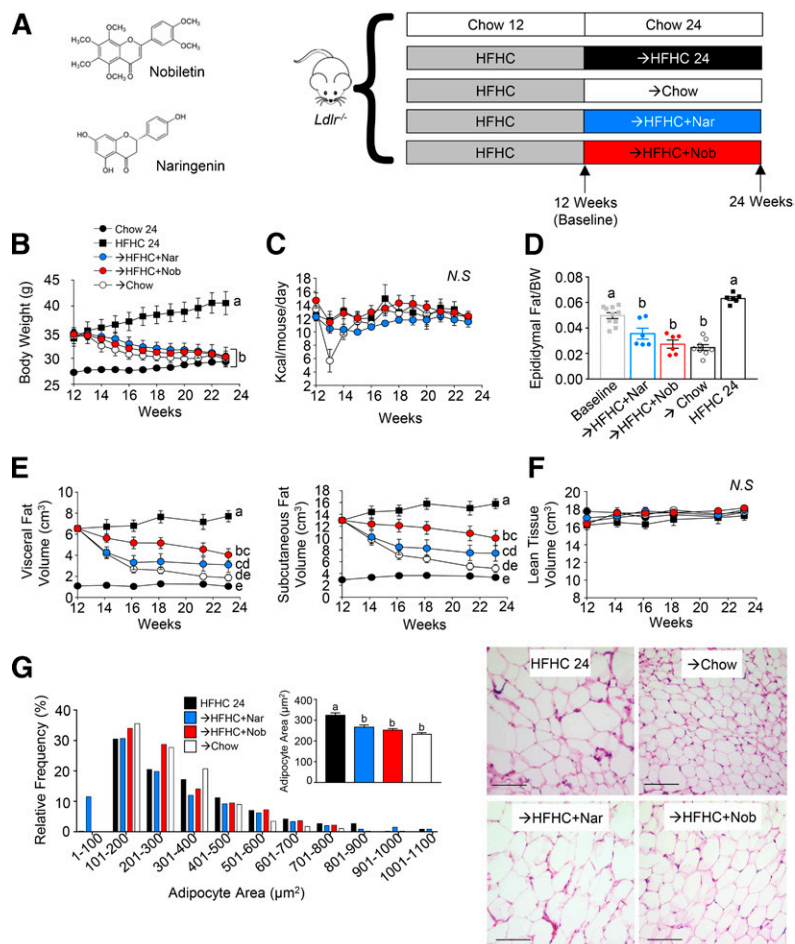
Fig. 1. Intervention with citrus flavonoids promotes weight loss and decreases adiposity. $Ldlr^{-/-}$ mice were fed a HFHC diet for 12 weeks. Subsequently, the same mice were treated with flavonoids added to the HFHC diet for an additional 12 weeks. A: Structure of naringenin (Nar) and nobiletin (Nob), and study design. B: Body weight measured weekly following intervention after induction (n = 6–10 per group). C: Caloric intake measured weekly during intervention (n = 6–10 per group). D: Adiposity assessed as epididymal fat pad weight/total body weight (n = 6–10 per group). E; Visceral and subcutaneous fat volume assessed by micro-CT (n = 6 per group). F: Lean tissue volume assessed by micro-CT (n = 6 per group). G: Frequency distribution of adipocyte area in mice at the end of intervention (n = 6 per group). Inset shows mean adipocyte area. Representative images of eWAT stained with H&E. Scale bar is 100 μm. Data represent the mean ± SEM. Different letters are statistically different by two-way ANOVA with post hoc Tukey test (B, C, E, F) and one-way ANOVA with post hoc Tukey test (D, G) ($P < 0.05$). N.S., not significant.

RER to ≥0.9 over 24 h, indicating enhanced oxidation of carbohydrates. In mice intervened with either flavonoid, food consumption increased by 2.5 kcal or ∼0.5 g per day, selectively in the dark cycle (Fig. 2C) and without changes in ambulatory activity (Fig. 2D). This small increase in food intake was not likely detectable when measured every 3 days in standard housing (Fig. 1C). Altogether, this suggests that flavonoid intervention enhanced energy expenditure and might induce a mild starvation response promoting greater food intake.

Flavonoid intervention normalizes insulin sensitivity

The ability of intervention with naringenin or nobiletin to reverse established insulin resistance was assessed. After induction with the HFHC diet, $Ldlr^{-/-}$ mice developed elevated fasting plasma insulin and mild hyperglycemia (**Fig. 3A**, B). Intervention with chow reversed hyperinsulinemia (−61%) and modestly improved hyperglycemia (−15%). The addition of either naringenin or nobiletin to the HFHC diet reversed hyperinsulinemia at week 24 by 50% and 54%, respectively, suggesting enhanced insulin sensitivity despite the concomitant HFHC diet (Fig. 3A). These significant reductions in fasting insulin levels were accompanied by decreases in fasting glucose by intervention with naringenin (−13%, trend) and nobiletin (−35%) (Fig. 3B). Temporally, improvements in fasting glucose were observed at 6 weeks of flavonoid intervention and were

maintained up to 12 weeks (Fig. 3C). HOMA-IR calculations showed that intervention with either flavonoid restored HOMA-IR to similar levels observed in chow-intervened mice (Fig. 3D). To determine whether normalized fasting insulin levels resulted in improved insulin or glucose tolerance, both tolerance tests were performed at baseline and after 12 weeks of intervention (Fig. 3E–J). At baseline, all groups had similar insulin tolerance or clearance of glucose shown as change in blood glucose concentration over time (Fig. 3E) and percent change in glucose over time (Fig. 3F). Following intervention, the lower fasting glucose levels in flavonoid-treated mice were accompanied by lower insulin tolerance test area under the plasma glucose curve [area under the curve (AUC)] (Fig. 3G), but there was no change in the efficiency of glucose clearance over time (Fig. 3H), suggesting that improved insulin tolerance did not enhance glucose clearance. Intervention with chow did not affect insulin tolerance (Fig. 3H). Similar glucose tolerance was observed in all groups following 12 weeks of induction (Fig. 3I). Intervention with the addition of either naringenin or nobiletin to the HFHC diet or with chow improved glucose tolerance compared with mice that remained on the HFHC diet alone (Fig. 3J). To understand peripheral insulin sensitivity further, we assessed muscle TG accumulation in quadriceps and gastrocnemii, which is known to impair insulin signaling (31) (Fig. 3K, L). The accumulation of TG in both the quadriceps and gastrocnemius
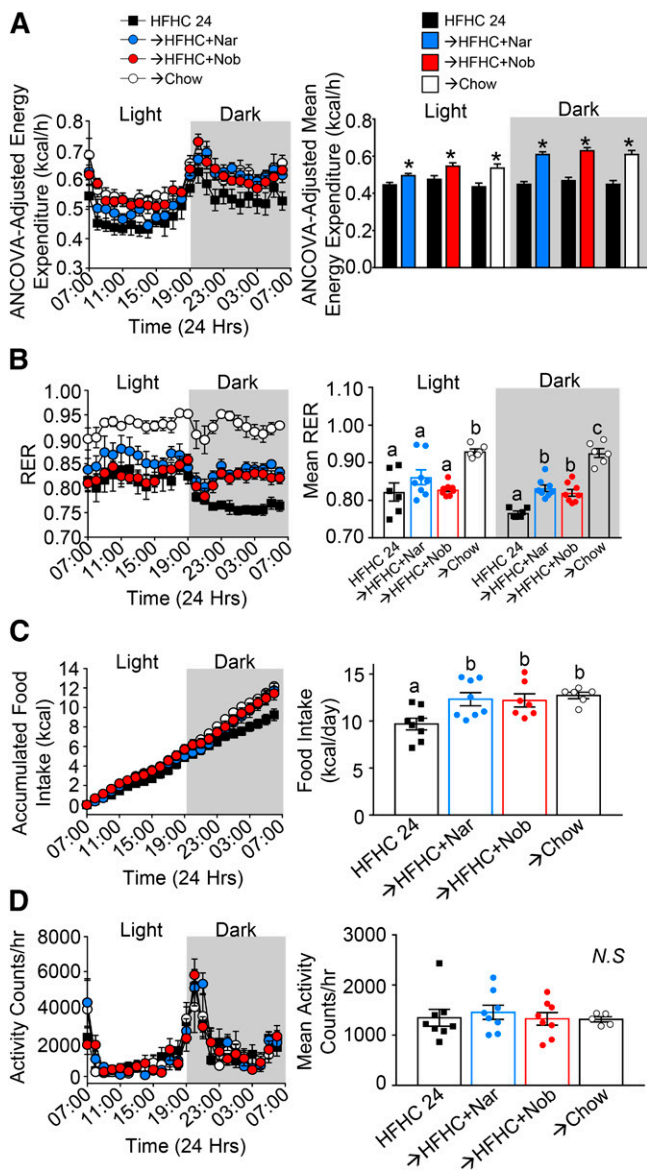
Fig. 2. Intervention with citrus flavonoids increases energy expenditure. $Ldlr^{-/-}$ mice were fed a HFHC diet for 12 weeks. Subsequently, the same mice were treated with flavonoids added to the HFHC diet for an additional 12 weeks. Between weeks 8 and 12 of intervention, mice were assessed in metabolic cages. A: ANCOVA-adjusted energy expenditure (kilocalories per hour) over 24 h and mean ANCOVA-adjusted energy expenditure in both the dark and light periods (n = 6–8 per group). B: RER over 24 h and mean RER in both the dark and light periods (n = 6–8 per group). C: Accumulated food intake over 24 h and total food eaten during 24 h (n = 6–8 per group). D: Ambulatory activity over 24 h and mean ambulatory activity per hour (n = 6–8 per group). Data represent the mean ± SEM. Different letters are statistically different by ANOVA with post hoc Tukey test ($P < 0.05$). *Indicates statistically significant by Student's t-test ($P < 0.05$). Nar, naringenin; Nob, nobiletin; N.S., not significant.

muscles was elevated at baseline and increased further by continuation on the HFHC diet (Fig. 3K, L). In quadriceps, intervention with naringenin, nobiletin, or chow reversed TG accumulation from baseline (Fig. 3K). In gastrocnemii, intervention with either flavonoid or chow decreased the mean TG levels from baseline (trend), but were

significantly lower compared with TG levels in HFHC-fed mice at 24 weeks (Fig. 3L).

Flavonoid intervention improves fatty liver

$Ldlr^{-/-}$ mice fed the HFHC induction diet accumulated both hepatic TGs and cholesterol (**Fig. 4A**–C). Compared with baseline, liver TG levels were reversed with intervention by either naringenin (-28%), nobiletin (-40%), or chow (-70%) (Fig. 4A). Compared with the HFHC diet at 24 weeks, intervention with either flavonoid or chow reduced liver TG by 58–82%. Compared with both baseline and HFHC at 24 weeks, liver CE and free cholesterol were lower with intervention by either naringenin (-70%, -40%), nobiletin (-60%, -33%), or chow (-90%, -53%), respectively (Fig. 4B, C). In prevention studies, we reported that a primary mechanism for flavonoid-induced reductions in liver lipids and associated metabolic abnormalities was enhanced $Pgc1a$- and $Cpt1a$-mediated fatty acid oxidation and attenuated $Srebp1c$-induced fatty acid synthesis (15, 16). In the present study, intervention with the addition of either naringenin or nobiletin to the HFHC diet reversed the HFHC diet-induced suppression of hepatic fatty acid oxidation, increasing it by 2-fold compared with baseline and by 1.4-fold compared with HFHC-fed mice at 24 weeks (Fig. 4D, E). This was accompanied by enhanced liver mRNA expression of $Cpt1a$ and $Pgc1a$. Improvements in hepatic lipids with flavonoid or chow intervention were associated with a reduction in $Srebf1c$ mRNA expression with naringenin (trend), nobiletin, and chow (Fig. 4E), suggesting reduced hepatic de novo lipogenesis. Liver weight was reduced with flavonoid treatment and there was no effect on hepatic $Acox1$ and $Ppara$ mRNA expression, indicating that the flavonoid effects were independent of peroxisome proliferation or activation of PPARα, consistent with our previous prevention studies (Fig. 4F; supplemental Fig. S4A, B) (16). Hepatic inflammation is also exacerbated by high-fat feeding (14). Intervention with either flavonoid in addition to HFHC completely normalized the mRNA expression of hepatic $Ccl2$, $Ccl3$, $Tnfa$, and $Il1b$, consistent with decreases in hepatic lipids and improvements in hepatic function (supplemental Fig. S4C–F).

Flavonoid intervention improves hyperlipidemia

Upon HFHC diet feeding, $Ldlr^{-/-}$ mice developed hypercholesterolemia and hypertriglyceridemia (**Fig. 5A–G**). Intervention with naringenin or nobiletin supplementation to the HFHC diet for 12 weeks reduced plasma cholesterol (>50%) and TGs (>50%) (Fig. 5A, B). Flavonoid-mediated plasma lipid lowering was confined to VLDL- and LDL-cholesterol with no change in HDL-cholesterol levels (Fig. 5C–H). Greater VLDL- and LDL-cholesterol reductions were observed with chow intervention (Fig. 5F, G).

Flavonoid intervention does not elicit atherosclerotic lesion contraction

Due to the significant improvement in atherosclerotic risk factors, we sought to determine the impact of flavonoid intervention on atherosclerosis regression. Aortic sinus lesions were assessed after HFHC induction (baseline) and
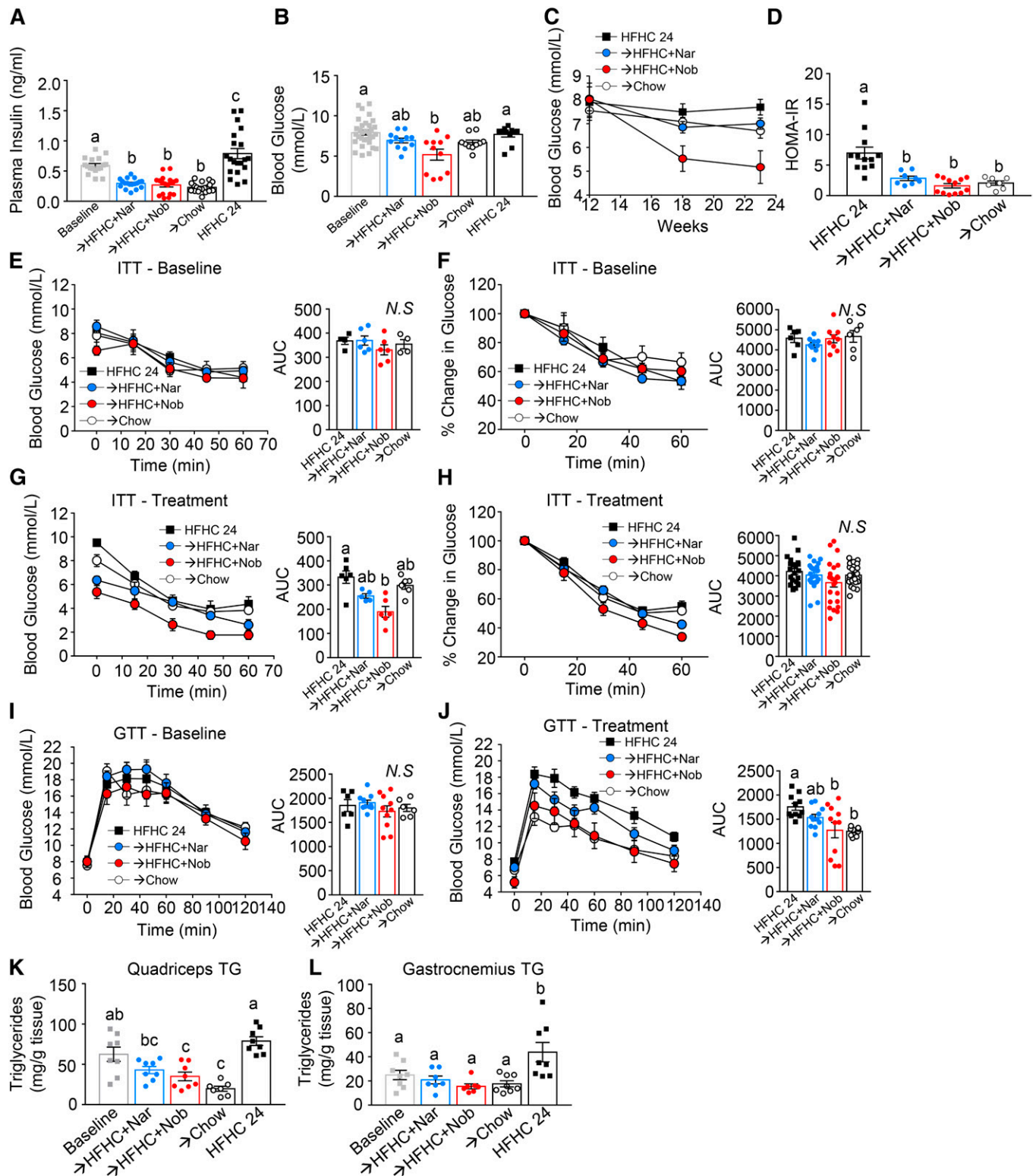
Fig. 3. Intervention with citrus flavonoids restores glucose homeostasis. $Ldlr^{-/-}$ mice were fed a HFHC diet for 12 weeks. Subsequently the same mice were treated with flavonoids added to the HFHC diet for an additional 12 weeks. A: Fasting (6 h) plasma insulin levels (n = 17–20 per group). B: Fasting (6 h) blood glucose (n = 10–32 per group). C: Fasting (6 h) blood glucose in the same mice at baseline and 6 weeks and 12 weeks of intervention (n = 11 per group). D: HOMA-IR (n = 7–12 per group). E, F: Insulin tolerance test (ITT) at baseline shown as blood glucose concentrations (n = 4–6 per group) (E) and percent change in glucose from time = 0 (n = 6–9 per group) (F). G, H; ITT at 12 weeks intervention shown as blood glucose concentrations (n = 5–6 per group) (G) and percent change in glucose from time = 0 (n = 22–24 per group) (H). I: Glucose tolerance test (GTT) at baseline (n = 6–9 per group). J: GTT at 12 weeks intervention (n = 10–11 per group). K, L: Muscle TG content in quadriceps (n = 8 per group) (K) and gastrocnemii and solei (n = 7–8 per group) (L). Data represent the mean ± SEM. Different letters are statistically different by ANOVA with post hoc Tukey test ($P < 0.05$). Nar, naringenin; Nob, nobiletin; N.S., not significant.
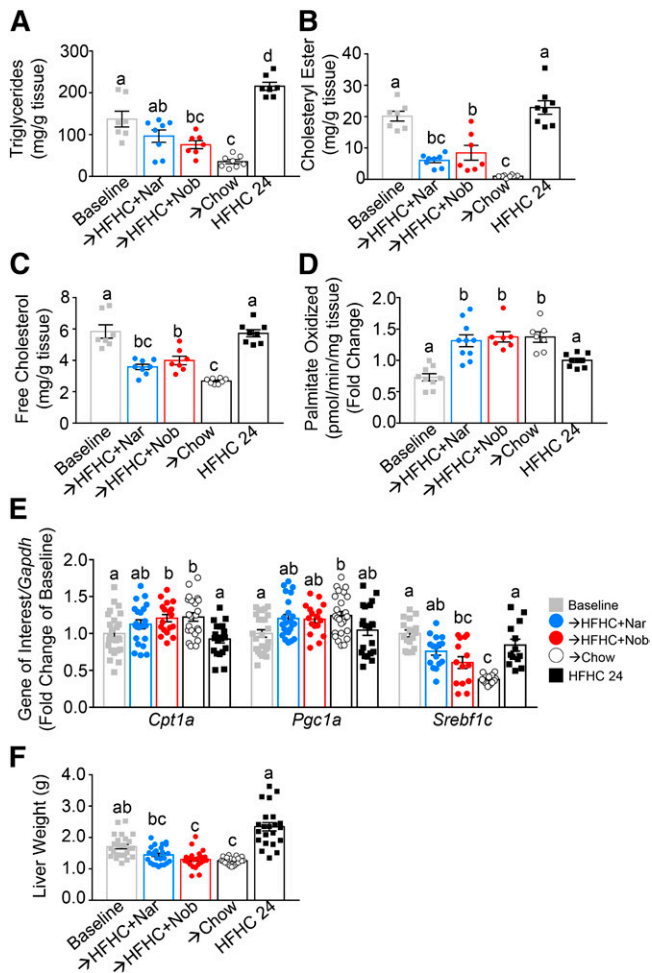
Fig. 4. Intervention with citrus flavonoids increases hepatic fatty acid oxidation and reduces liver steatosis. $Ldlr^{-/-}$ mice were fed a HFHC diet for 12 weeks. Subsequently, the same mice were treated with flavonoids added to the HFHC diet for an additional 12 weeks. A: Hepatic TGs (n = 7–8 per group). B: Hepatic CE (n = 7–8 per group). C: Hepatic free cholesterol (n = 7–8 per group). D: Ex vivo hepatic fatty acid oxidation (n = 7–10 per group). E: Hepatic gene expression (n = 12 per group). F: Liver weight (n = 22 per group). Data represent the mean ± SEM. Different letters are statistically different by ANOVA with post hoc Tukey test ($P < 0.05$). Nar, naringenin; Nob, nobiletin.

following flavonoid or chow intervention (**Fig. 6A**). While intervention with chow did not induce regression of aortic sinus lesions, their growth in size was significantly attenuated. Intervention with either citrus flavonoid to the HFHC diet did not affect lesion size; the area of sinus lesions continued to increase at the same rate as in mice fed the HFHC diet alone for 24 weeks (Fig. 6A). Lipid measurements in whole aortae, dissected free from fat, revealed that the aortae of HFHC-fed mice continued to accumulate free cholesterol and CE (~4-fold) compared with baseline (Fig. 6B). The addition of either flavonoid at intervention slowed, but did not halt, the accumulation of aortic free or esterified cholesterol (Fig. 6B). Chow intervention prevented further increases from baseline in aortic cholesterol content. The aortic mRNA expression of the inflammatory genes, *Ccl3*, *Tnfa*, and *Emr1*, increased from baseline with continued HFHC, which was not offset by flavonoid
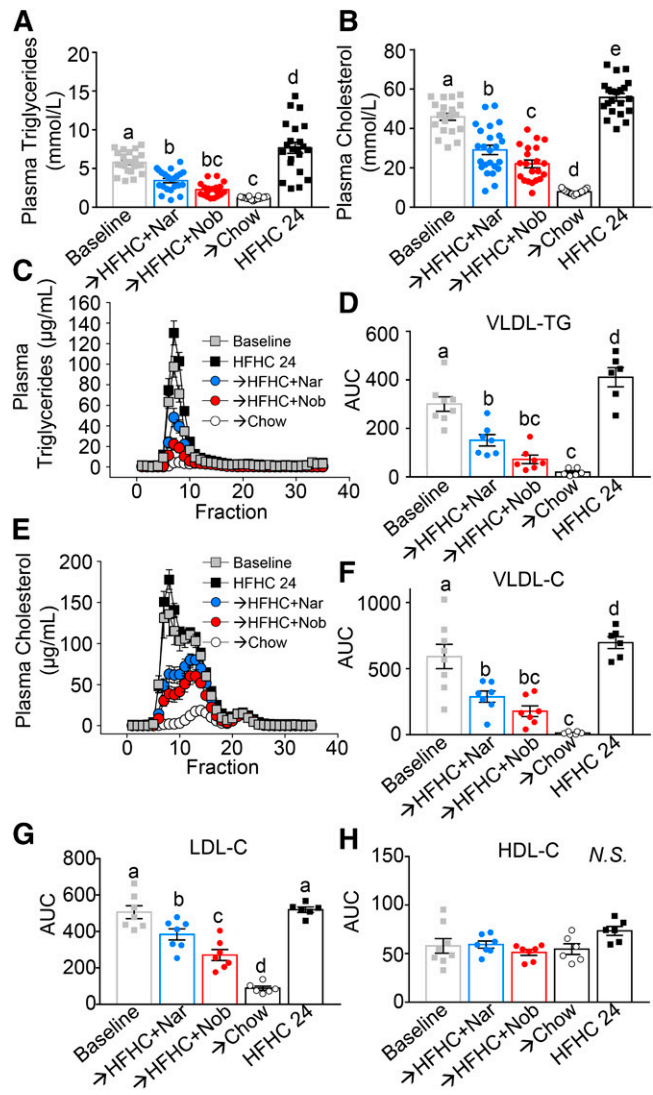

Fig. 5. Intervention with citrus flavonoids lowers plasma lipids from baseline. $Ldlr^{-/-}$ mice were fed a HFHC diet for 12 weeks. Subsequently, the same mice were treated with flavonoids added to the HFHC diet for an additional 12 weeks. Mice were fasted for 6 h prior to euthanization. Plasma was subjected to FPLC and lipids were measured in each fraction by enzymatic assay. A: Plasma TGs (n = 19–24 per group). B: Plasma cholesterol (C) (n = 21–24 per group). C: Plasma TG FPLC tracing (n = 6–7 per group). D: Plasma VLDL TG AUC calculations (n = 6–7 per group). E: Plasma cholesterol FPLC tracing (n = 6–7 per group) F: Plasma VLDL cholesterol AUC calculations (n = 6–7 per group). G: Plasma LDL cholesterol AUC calculations (n = 6–7 per group). H: Plasma HDL cholesterol AUC calculations (n = 6–7 per group. Data represent the mean ± SEM. Different letters are statistically different by ANOVA with post hoc Tukey test ($P < 0.05$). Nar, naringenin; Nob, nobiletin; N.S., not significant.

intervention (Fig. 6C). Aortic mRNA of *Il1b* and *Ccl2* were not different from baseline in mice continued on HFHC or with flavonoid intervention. Chow intervention tended to halt or reverse aortic mRNA expression of all inflammatory markers examined (Fig. 6C). Additionally, intervention with either flavonoid did not increase the expression of genes linked to regression and chow intervention actually decreased the mRNA expression of *Ccr7*, *Abca1*, and *Abcg1* (Fig. 6C).
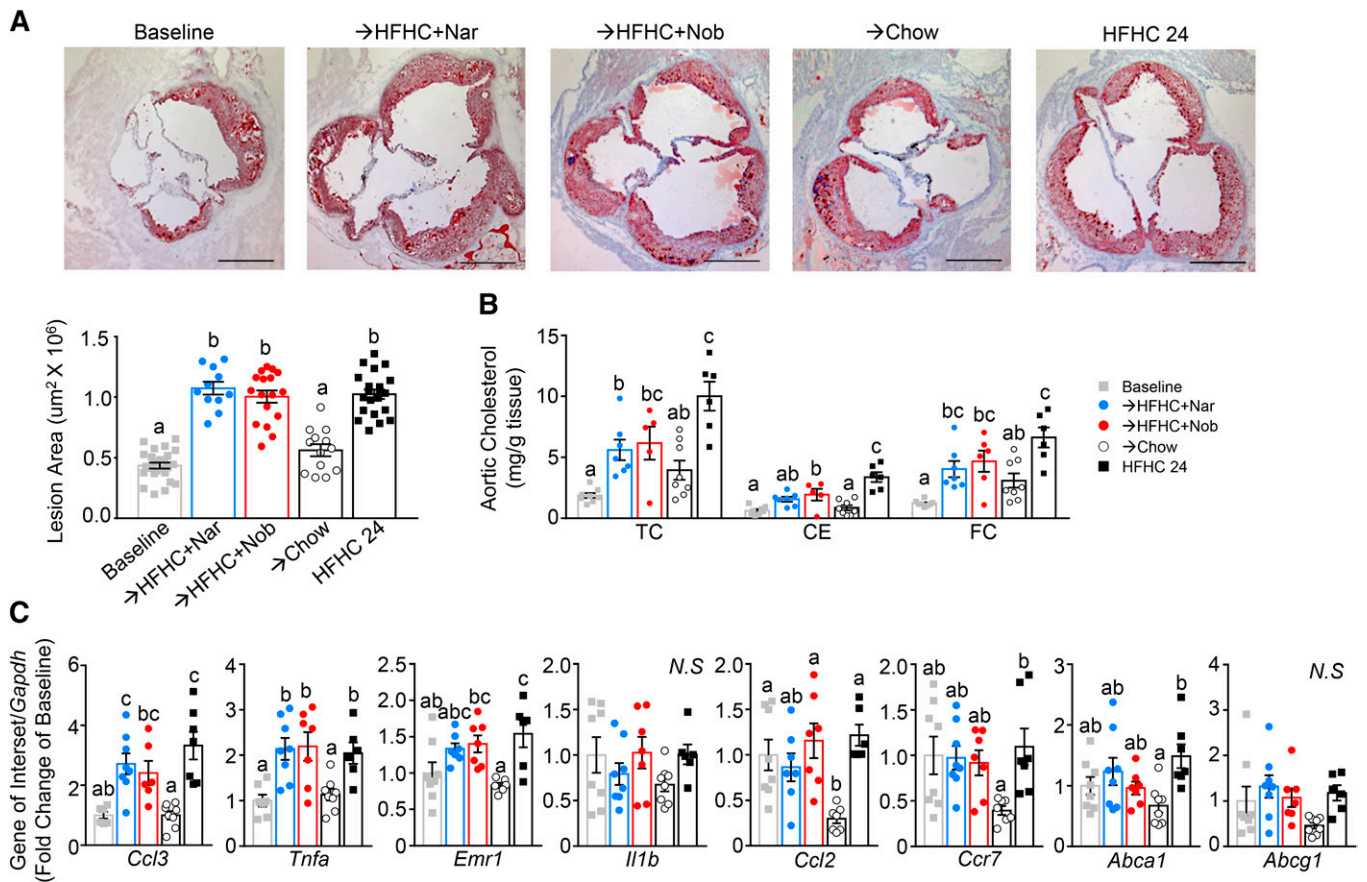
Fig. 6. Intervention with citrus flavonoids does not attenuate lesion size but slows aortic cholesterol accumulation. $Ldlr^{-/-}$ mice were fed a HFHC diet for 12 weeks. Subsequently, the same mice were treated with flavonoids added to the HFHC diet for an additional 12 weeks. Aortae were dissected and the aortic sinus sectioned and analyzed histologically. A: Representative sections of the aortic sinus stained with oil red-O and hematoxylin and lesion area quantitation (n = 12–21 per group). Scale bar is 500 μm. B: Total cholesterol (TC), cholesteryl ester CE, and free cholesterol (FC) in whole aortae (n = 6–8 per group). C: Gene expression in whole aortae (n = 6–8 per group). Data represent the mean ± SEM. Different letters are statistically different by ANOVA with post hoc Tukey test ($P < 0.05$). Nar, naringenin; Nob, nobiletin; N.S., not significant.

Flavonoid intervention reduces plaque macrophages

Although there was no change in the plaque size with flavonoid intervention, the decrease in aortic cholesterol suggested that lesion composition may have been favorably altered (Fig. 6A, B). After 12 weeks induction, plaques were comprised mainly of macrophages (~66%) (**Fig. 7A**, H). Lesion macrophage content was reduced with intervention by naringenin (−47%), nobiletin (−50%), and chow (−69%) (Fig. 7A, H), consistent with the concept that depletion of macrophages is characteristic of a regressing plaque (21). Although the percent of lesion area occupied by macrophages was also less in mice continuing on HFHC (−23%), the decrease was greater with flavonoid or chow intervention (Fig. 7A, H). Compared with lesions at baseline, continuation on the HFHC diet enlarged necrotic core area (from 6% to 14%), increased the percent of apoptotic cells (from 0.2% to 1.0%), reduced lesion smooth muscle cells (SMCs) (from 3.5% to 1.8%), and increased lesion collagen (from 20% to 35%) (Fig. 7B–F, Supplemental Fig. S5). Intervention with either naringenin, nobiletin, or chow halted the increase in necrotic core size, inhibited the increase in apoptosis, attenuated the decrease in SMCs, and maintained the increase in lesion collagen (Fig. 7B–F,

supplemental Fig. S5). Collectively, these intervention-induced changes in lesion composition are characteristic of more stable lesions (Fig. 7G).

Flavonoid intervention prevents enhanced monocytosis

Reduced plaque macrophage content is phenotypically associated with atherosclerosis regression (21, 32–34). Reduced monocyte recruitment from the circulation has been implicated as a mechanism contributing to regression (29). In this study, continuation of the HFHC diet increased the number of circulating Ly6C^{hi} monocytes (2-fold) (**Fig. 8A**), the monocyte subset known to be the precursor of lesion M1 and M2 macrophages (35). Intervention with chow or nobiletin completely prevented the increase in Ly-6C^{hi} monocytes, while with naringenin intervention, there was a trend to attenuation of the HFHC-induced elevation in Ly6C^{hi} monocytes (Fig. 8A). There was no effect on circulating Ly6C^{lo} monocytes or total neutrophil levels with continuation of the HFHC diet or with any intervention (Fig. 8B, D). To investigate this trend further, bone marrow progenitor populations were measured (supplemental Fig. S6). Intervention with chow reduced bone marrow hematopoietic stem and progenitor cell populations, whereas
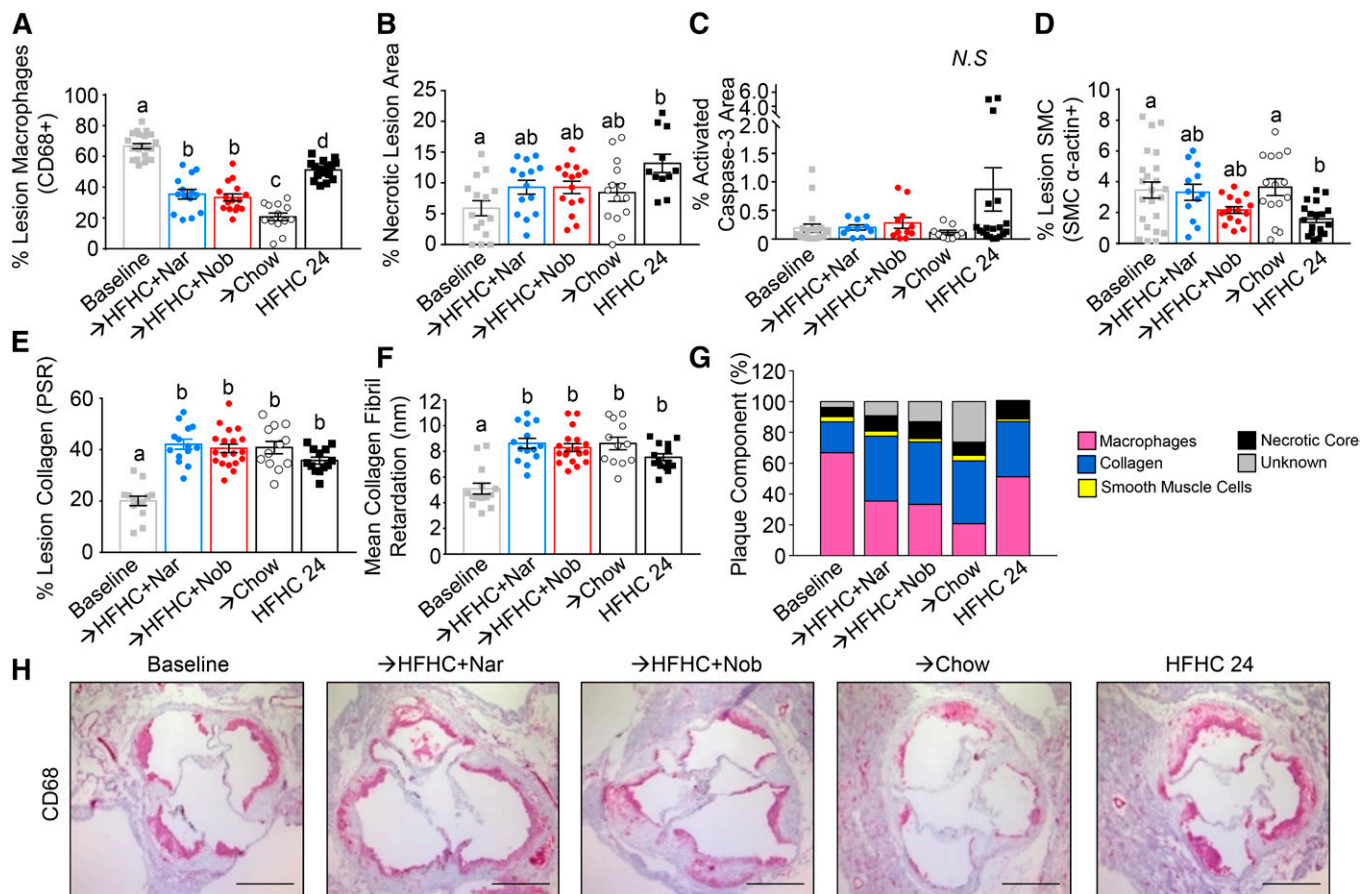
Fig. 7. Intervention with citrus flavonoids improves lesion morphology. $Ldlr^{-/-}$ mice were fed a HFHC diet for 12 weeks. Subsequently, the same mice were treated with flavonoids added to the HFHC diet for an additional 12 weeks. Aortae were dissected and the aortic sinus sectioned and analyzed histologically. A: Percent of lesion area occupied by CD68+ macrophages (n = 14–22 per group). B: Percent of lesion area occupied by the necrotic core (n = 14–17). C: Percent of lesion positive for activated capase-3 (n = 9–20 per group). D: Percent of lesion area occupied by SMCs (α-actin) (n = 12–23 per group). E: Percent of lesion area occupied by collagen (picrosirius red) (n = 12–19 per group). F: Collagen organization measured as mean collagen fibril retardation (n = 12–19 per group). G: Lesion composition for each dietary group. H: Representative histological sections of the aortic sinus stained with CD68 (macrophages) and counterstained with hematoxylin. Scale bar is 500 μm. Data represent the mean ± SEM. Different letters are statistically different by ANOVA with post hoc Tukey test ($P < 0.05$). Nar, naringenin; Nob, nobiletin; N.S., not significant.

the modest reductions with flavonoid intervention were not significant (supplemental Fig. S6A, C). A similar trend persisted when looking at bone marrow myeloid progenitor cells (supplemental Fig. S6B, C), common myeloid progenitor cells (supplemental Fig. S6D, G), and granulocyte macrophage progenitor cells (supplemental Fig. S6E, G). There was no consistent effect of any treatment group on megakaryocyte and erythrocyte progenitor cells (supplemental Fig. S6F, G).

DISCUSSION

In the present study, we showed that intervention with the citrus-derived flavonoids, naringenin or nobiletin, when supplemented to a HFHC diet, reversed diet-induced obesity and insulin resistance, improved hyperlipidemia and hepatic steatosis, and favorably altered aortic sinus atherosclerotic plaque composition. Flavonoid intervention enhanced energy expenditure, despite promoting a modest increase in food consumption during the active time

and while maintaining similar ambulatory activity. In the liver, fatty acid oxidation was increased, as were *Cpt1a* and *Pgc1a* expression, suggesting enhanced fat mobilization. In white adipose tissue, there were no consistent effects on browning genes in visceral or subcutaneous depots and no enhancement of browning genes in BAT, suggesting a non-browning mechanism of enhanced energy expenditure and reduced adiposity. Although atherosclerotic lesion size was unaffected, the improvements in metabolic parameters with flavonoid intervention correlated with a reduction in circulating monocytes and reduced macrophage content in established atherosclerotic lesions, characteristics consistent with atherosclerosis regression (22).

Changes in food consumption can result from the effects of dietary components or drugs on behavior, satiety, or energy balance, which in turn alter metabolic regulation, including adipose tissue metabolism (30). Consistent with previously reported prevention studies, addition of flavonoids to the HFHC diet did not decrease caloric intake as measured in standard caging (13–16). Studies from other laboratories have reported reduced caloric intake in
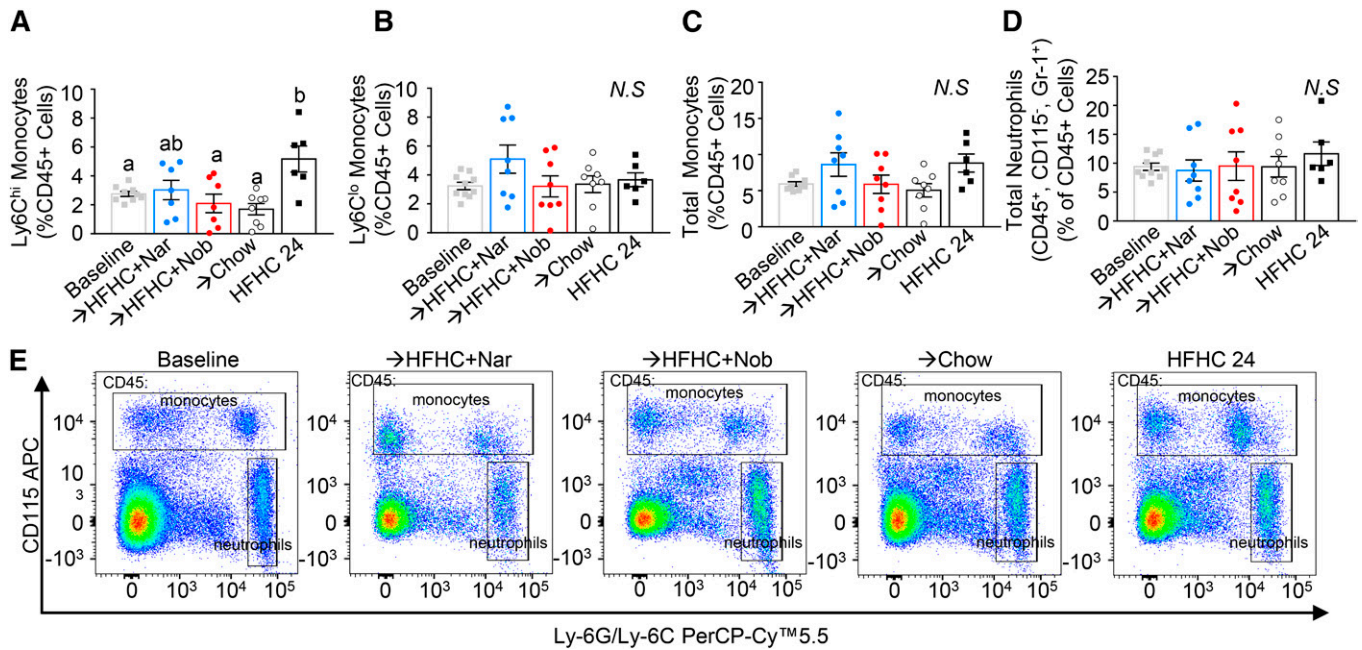
Fig. 8. Intervention with citrus flavonoids prevents further elevation in blood monocytes. $Ldlr^{-/-}$ mice were fed a HFHC diet for 12 weeks. Subsequently the same mice were treated with flavonoids added to the HFHC diet for an additional 12 weeks. Peripheral blood mononuclear cells (PBMCs) were isolated and stained for monocyte and neutrophil markers. A: Percent PBMCs that were Ly6C^{hi} monocytes (n = 9–10 per group). B: Percent of PBMCs that were Ly6C^{lo} monocytes (n = 9–10 per group). C: Percent of PBMCs that were both Ly6C^{hi} and Ly6C^{lo} monocytes. D: Percent of PBMCs that were neutrophils. E: Representative flow cytometric pseudocolor plots show monocytes and neutrophil populations from each dietary group. Data represent the mean ± SEM. Different letters are statistically different by ANOVA with post hoc Tukey test ($P < 0.05$). Nar, naringenin; Nob, nobiletin; N.S., not significant.

high-fat-fed mice with naringenin intervention, leading to decreased body weight and adiposity (36), an effect likely attributed to a taste aversion to the compound when administered in the food. In the present study, taste aversion was mitigated by starting intervention at a low flavonoid dose, which was slowly increased to the final dose over the first week of intervention. Thus, food intake did not drop precipitously, which would in itself cause weight loss. In metabolic cage studies, we unexpectedly identified a small (~0.5 g/day) but significant increase in caloric consumption during the dark cycle in both naringenin- and nobiletin-treated mice, at weeks 21–23, near the end of the intervention. Despite this small increase, intervention with both flavonoids induced weight loss, decreased adiposity, and improved metabolic indices, implying the molecular mechanism for the flavonoid effects was not related to suppressed food intake (30). The reasons underlying the flavonoid-induced increase in caloric intake during the dark cycle is not well understood, but may be related to a mild starvation response resulting from increased energy expenditure. Pair-feeding experiments would help to confirm and further understand this observation.

Naringenin intervention has previously been studied in ovariectomized female C57BL/6J mice to assess its impact on postmenopausal metabolic dysfunction (36, 37). In chow-fed ovariectomized mice at a normal body weight, intervention by the addition of naringenin to chow prevented weight gain while promoting modest weight loss, reduced adiposity, and improved glucose homeostasis, accompanied by a reduction in caloric intake (36). When the same

ovariectomized mice were fed a high-fat diet, intervention with the addition of naringenin to the high-fat diet prevented further weight gain and adiposity, while increasing ambulatory activity, with no change in energy expenditure (37). In our male $Ldlr^{-/-}$ mice fed a high-fat diet, intervention with either flavonoid also decreased body weight and adiposity, but was due to an increase in ANCOVA-adjusted energy expenditure, with no change in ambulatory activity and despite a small increase in caloric intake. Ambulatory activity was lower in treated postmenopausal mice compared with our flavonoid-intervention in $Ldlr^{-/-}$ mice, which might be attributed to postmenopausal sarcopenia. It is possible that the discrepancy in activity results could be due to differences in age and sex of the two models. The lack of effect of flavonoid intervention on activity is consistent with our previous prevention studies in high-fat-fed $Ldlr^{-/-}$ mice treated with both naringenin and nobiletin (15, 16). Experiments in age-matched female $Ldlr^{-/-}$ mice would help to further understand this observation.

Hypercholesterolemia, hyperglycemia, obesity, and, more specifically, adipose tissue inflammation are all independent risk factors for leukocytosis, which can contribute to accelerated atherosclerosis (32, 38, 39). In the present study, intervention with either naringenin or nobiletin reduced atherosclerotic lesion macrophage content, consistent with plaque regression. Reduced monocyte recruitment to atherosclerotic plaques is characteristic of atherosclerosis regression (21, 34). While trafficking kinetics to determine the contribution of monocyte recruitment to the reduced lesion macrophage content were not performed, leukocyte

levels in the circulation were quantitated. Intervention with naringenin or nobiletin prevented any further increase in circulating Ly6C^{hi} monocytes, known to be the precursor of lesion macrophages (35). We also showed that intervention with chow induced a more notable, but not significant, reduction from baseline in blood Ly6C^{hi} monocytes compared with flavonoid intervention, but this did not translate into a reduction in circulating total monocytes. This chow-alone intervention effect is consistent with previous regression studies in high-fat-fed $Ldlr^{-/-}$ mice (32), but not studies in high-fat-fed $Ldlr^{-/-}$ mice in which the chow intervention was coupled to hepatic $Mttp$ deletion, which resulted in more rapid regression and a large reduction in circulating monocytes (33). It is possible that interventions with dietary flavonoids plus HFHC or chow alone were not strong enough or long enough in duration to achieve larger significant reductions in circulating monocytes (32, 33). In addition, neither flavonoid nor chow intervention completely corrected hypercholesterolemia, thereby restricting a more robust reduction in myelopoiesis (38). Furthermore, we used $Ldlr^{-/-}$ mice, which develop more modest monocytosis compared with $Apoe^{-/-}$ mice in response to a high-fat diet, which would make the effects of naringenin or nobiletin intervention more subtle, especially considering the incomplete correction of metabolic dysfunction (29).

The mechanism(s) through which either naringenin or nobiletin regulate energy expenditure, lipid metabolism, and insulin sensitivity are not completely understood. Previous in vitro studies demonstrated that both naringenin and nobiletin activate insulin signaling independent of the insulin receptor or insulin receptor substrate (16, 40). Additionally, in high-fat-fed $Ldlr^{-/-}$ mice, both naringenin and nobiletin upregulated $Pcg1\alpha$- and $Cpt1\alpha$-mediated hepatic fatty acid oxidation, independent of peroxisomal proliferation, and suppressed $Srebp1c$-mediated fatty acid synthesis (15, 16). The upstream mechanism(s) governing these effects have remained somewhat elusive. The hormone-like fibroblast growth factor 21 elicits similar metabolic improvements as naringenin when given exogenously to mice, but naringenin prevented metabolic dysfunction and obesity in high-fat-fed $Fgf21^{-/-}$ mice to the same extent as in wild-type mice (13). In short-term treatment of Ob/Ob mice, naringenin supplementation to a low-fat diet reversed hyperlipidemia, attenuated body weight, and improved hepatic steatosis and insulin sensitivity, indicating that the naringenin effect was independent of leptin deficiency (13). This suggests that, unlike other natural compounds, such as celastrol and withaferin A, naringenin does not work through enhancing leptin sensitivity (41, 42). Alternatively, celastrol has also been shown to prevent weight gain and improve metabolic dysfunction through activation of the heat shock factor 1-PGC1α axis in adipose tissue and muscle, but not liver (43), more similar to, but not identical to, the hepatic effects of naringenin or nobiletin.

Recent studies revealed that the addition of naringenin plus apigenin (a related flavonoid) to a high-fat diet prevented the exacerbated rebound in body weight in mice, when rechallenged with a high-fat diet following a period of chow-induced weight loss (44). Celastrol or a leptin-sensitizing antagonist did not mitigate weight rebound. Flavonoid treatment replaced the persistent high-fat diet-induced loss of microbiome-derived flavonoid availability, resulting in increased energy expenditure and upregulation of $Ucp1$ expression in BAT (44). In prevention models, we have shown that naringenin modestly increases $Ucp1$ expression in iWAT (13); but in the present study, we saw no effect with either naringenin or nobiletin on iWAT or BAT $Ucp1$ expression. Additionally, we reported no change with nobiletin treatment on nonshivering thermogenesis; however, experiments were not conducted at thermoneutrality (16). This suggests that flavonoid-mediated enhanced browning may not be the mechanism through which citrus flavonoids exert their anti-obesity effects. It is possible that the browning effect of flavonoids in the weight cycling mouse model was apigenin specific. Nobiletin, but not naringenin, has been shown to enhance the amplitude of circadian rhythms, specifically in obese mice (45). In our previous studies, we have not observed any differences in the effects of either naringenin or nobiletin treatment aside from potency. Nobiletin is ~10 times more potent than naringenin, which is reflected in its lower effective dose (0.3% vs. 3% of diet) (15, 16). It is possible that naringenin may also enhance clock sensitivity and that differences in dosing and administration may be responsible for the discrepancy in results between naringenin and nobiletin (15, 45).

In the present study, we tested one protocol of induction and intervention times, 12 weeks induction with a HFHC diet followed by 12 weeks intervention with either citrus flavonoid supplemented to the HFHC diet. These timelines were chosen based on atherosclerosis regression models in the literature and are similar to other dietary flavonoid-intervention timelines (21, 36, 37). Twelve weeks of HFHC induction was sufficient time to induce moderate obesity, significant hyperlipidemia, moderate insulin resistance, hepatic steatosis, and intermediate atherosclerosis. Twelve weeks intervention was sufficient to completely improve obesity and insulin resistance, but moderate hyperlipidemia and hepatic steatosis persisted, resulting in improvements in lesion morphology, but no regression of plaque size. This raises the intriguing possibility that a longer duration of flavonoid intervention would result in greater resolution of these disorders. It would be of interest to test different intervention durations and potentially longer induction periods to test the limits of flavonoid intervention on the resolution of diet-induced obesity, metabolic syndrome, and atherosclerosis.

A number of human studies using purified citrus flavonoids have demonstrated improvements in plasma lipids, glucose metabolism, and obesity [reviewed in (11)]. However, results were modest and inconsistencies between studies and considerable inter-patient variation were observed. Bioavailability of flavonoids is low, especially in humans; metabolism of flavonoids differs between subjects and differences in the enteric microflora may be responsible for considerable inter-individual variability in absorption and pharmacokinetic parameters (11). Larger controlled

human studies are required to assess dose, bioavailability, efficacy, and safety for therapeutic development.

In summary, we have shown that intervention by the addition of either of the citrus flavonoids, naringenin or nobiletin, to a high-fat diet in obese mice reverses weight gain and adiposity similar to intervention with chow, without reducing food intake. Mice treated with naringenin or nobiletin consume more calories, but expend more energy without increased ambulatory activity. Flavonoid-treated mice regain insulin sensitivity and reverse hyperinsulinemia completely. Plasma lipids are decreased and hepatic fatty acid oxidation is increased resulting in reduced hepatic lipids. Collectively these improvements in atherogenic risk factors did not result in lesion contraction, but improved lesion morphology, most notably reduced lesion macrophage content, consistent with early stages of atherosclerosis regression. These studies highlight the potential therapeutic utility of either naringenin or nobiletin, especially in the context of existing obesity and metabolic dysfunction.■

REFERENCES

1. Hamilton, M. T., D. G. Hamilton, and T. W. Zderic. 2007. Role of low energy expenditure and sitting in obesity, metabolic syndrome, type 2 diabetes, and cardiovascular disease. *Diabetes.* **56:** 2655–2667.
2. Olshansky, S. J., D. J. Passaro, R. C. Hershow, J. Layden, B. A. Carnes, J. Brody, L. Hayflick, R. N. Butler, D. B. Allison, and D. S. Ludwig. 2005. A potential decline in life expectancy in the United States in the 21st century. *N. Engl. J. Med.* **352:** 1138–1145.
3. Saltiel, A. R. 2016. New therapeutic approaches for the treatment of obesity. *Sci. Transl. Med.* **8:** 323rv2.
4. Rodgers, R. J., M. H. Tschop, and J. P. Wilding. 2012. Anti-obesity drugs: past, present and future. *Dis. Model. Mech.* **5:** 621–626.
5. Heymsfield, S. B., and T. A. Wadden. 2017. Mechanisms, pathophysiology, and management of obesity. *N. Engl. J. Med.* **376:** 254–266.
6. Khera, R., M. H. Murad, A. K. Chandar, P. S. Dulai, Z. Wang, L. J. Prokop, R. Loomba, M. Camilleri, and S. Singh. 2016. Association of pharmacological treatments for obesity with weight loss and adverse events: a systematic review and meta-analysis. *JAMA.* **315:** 2424–2434.
7. Adams, T. D., L. E. Davidson, S. E. Litwin, J. Kim, R. L. Kolotkin, M. N. Nanjee, J. M. Gutierrez, S. J. Frogley, A. R. Ibele, E. A. Brinton, et al. 2017. Weight and metabolic outcomes 12 years after gastric bypass. *N. Engl. J. Med.* **377:** 1143–1155.
8. Nguyen, N. T., and J. E. Varela. 2017. Bariatric surgery for obesity and metabolic disorders: state of the art. *Nat. Rev. Gastroenterol. Hepatol.* **14:** 160–169.
9. Eckel, R. H., S. M. Grundy, and P. Z. Zimmet. 2005. The metabolic syndrome. *Lancet.* **365:** 1415–1428.
10. Wilson, P. W., R. B. D'Agostino, L. Sullivan, H. Parise, and W. B. Kannel. 2002. Overweight and obesity as determinants of cardiovascular risk: the Framingham experience. *Arch. Intern. Med.* **162:** 1867–1872.
11. Mulvihill, E. E., A. C. Burke, and M. W. Huff. 2016. Citrus flavonoids as regulators of lipoprotein metabolism and atherosclerosis. *Annu. Rev. Nutr.* **36:** 275–299.
12. Amiot, M. J., C. Riva, and A. Vinet. 2016. Effects of dietary polyphenols on metabolic syndrome features in humans: a systematic review. *Obes. Rev.* **17:** 573–586.
13. Assini, J. M., E. E. Mulvihill, A. C. Burke, B. G. Sutherland, D. E. Telford, S. S. Chhoker, C. G. Sawyez, M. Drangova, A. C. Adams, A. Kharitonenkov, et al. 2015. Naringenin prevents obesity, hepatic steatosis, and glucose intolerance in male mice independent of fibroblast growth factor 21. *Endocrinology.* **156:** 2087–2102.
14. Assini, J. M., E. E. Mulvihill, B. G. Sutherland, D. E. Telford, C. G. Sawyez, S. L. Felder, S. Chhoker, J. Y. Edwards, R. Gros, and M. W. Huff. 2013. Naringenin prevents cholesterol-induced systemic inflammation, metabolic dysregulation, and atherosclerosis in *Ldlr-/-* mice. *J. Lipid Res.* **54:** 711–724.
15. Mulvihill, E. E., E. M. Allister, B. G. Sutherland, D. E. Telford, C. G. Sawyez, J. Y. Edwards, J. M. Markle, R. A. Hegele, and M. W. Huff. 2009. Naringenin prevents dyslipidemia, apolipoprotein B overproduction, and hyperinsulinemia in LDL receptor-null mice with diet-induced insulin resistance. *Diabetes.* **58:** 2198–2210.
16. Mulvihill, E. E., J. M. Assini, J. K. Lee, E. M. Allister, B. G. Sutherland, J. B. Koppes, C. G. Sawyez, J. Y. Edwards, D. E. Telford, A. Charbonneau, et al. 2011. Nobiletin attenuates VLDL overproduction, dyslipidemia, and atherosclerosis in mice with diet-induced insulin resistance. *Diabetes.* **60:** 1446–1457.
17. Mulvihill, E. E., J. M. Assini, B. G. Sutherland, A. S. DiMattia, M. Khami, J. B. Koppes, C. G. Sawyez, S. C. Whitman, and M. W. Huff. 2010. Naringenin decreases progression of atherosclerosis by improving dyslipidemia in high-fat-fed low-density lipoprotein receptor-null mice. *Arterioscler. Thromb. Vasc. Biol.* **30:** 742–748.
18. Borradaile, N. M., L. E. de Dreu, and M. W. Huff. 2003. Inhibition of net HepG2 cell apolipoprotein B secretion by the citrus flavonoid naringenin involves activation of phosphatidylinositol 3-kinase, independent of insulin receptor substrate-1 phosphorylation. *Diabetes.* **52:** 2554–2561.
19. Whitman, S. C., E. M. Kurowska, J. A. Manthey, and A. Daugherty. 2005. Nobiletin, a citrus flavonoid isolated from tangerines, selectively inhibits class A scavenger receptor-mediated metabolism of acetylated LDL by mouse macrophages. *Atherosclerosis.* **178:** 25–32.
20. Lin, N., T. Sato, Y. Takayama, Y. Mimaki, Y. Sashida, M. Yano, and A. Ito. 2003. Novel anti-inflammatory actions of nobiletin, a citrus polymethoxy flavonoid, on human synovial fibroblasts and mouse macrophages. *Biochem. Pharmacol.* **65:** 2065–2071.
21. Burke, A. C., and M. W. Huff. 2018. Regression of atherosclerosis: lessons learned from genetically modified mouse models. *Curr. Opin. Lipidol.* **29:** 87–94.
22. Basu, D., Y. Hu, L. A. Huggins, A. E. Mullick, M. J. Graham, T. Wietecha, S. Barnhart, A. Mogul, K. Pfeiffer, A. Zirlik, et al. 2018. Novel reversible model of atherosclerosis and regression using oligonucleotide regulation of the LDL receptor. *Circ. Res.* **122:** 560–567.
23. Granton, P. V., C. J. Norley, J. Umoh, E. A. Turley, B. C. Frier, E. G. Noble, and D. W. Holdsworth. 2010. Rapid in vivo whole body composition of rats using cone beam muCT. *J. Appl. Physiol. (1985).* **109:** 1162–1169.
24. Luu, Y. K., S. Lublinsky, E. Ozcivici, E. Capilla, J. E. Pessin, C. T. Rubin, and S. Judex. 2009. In vivo quantification of subcutaneous and visceral adiposity by micro-computed tomography in a small animal model. *Med. Eng. Phys.* **31:** 34–41.
25. Folch, J., M. Lees, and G. H. Sloane Stanley. 1957. A simple method for the isolation and purification of total lipides from animal tissues. *J. Biol. Chem.* **226:** 497–509.
26. Murakami, N., T. Ohtsubo, Y. Kansui, K. Goto, H. Noguchi, Y. Haga, Y. Nakabeppu, K. Matsumura, and T. Kitazono. 2014. Mice heterozygous for the xanthine oxidoreductase gene facilitate lipid accumulation in adipocytes. *Arterioscler. Thromb. Vasc. Biol.* **34:** 44–51.
27. Huss, J. M., I. P. Torra, B. Staels, V. Giguere, and D. P. Kelly. 2004. Estrogen-related receptor alpha directs peroxisome proliferator-activated receptor alpha signaling in the transcriptional control of energy metabolism in cardiac and skeletal muscle. *Mol. Cell. Biol.* **24:** 9079–9091.
28. Bojic, L. A., A. C. Burke, S. S. Chhoker, D. E. Telford, B. G. Sutherland, J. Y. Edwards, C. G. Sawyez, R. G. Tirona, H. Yin, J. G. Pickering, et al. 2014. Peroxisome proliferator-activated receptor delta agonist GW1516 attenuates diet-induced aortic inflammation, insulin resistance, and atherosclerosis in low-density lipoprotein receptor knockout mice. *Arterioscler. Thromb. Vasc. Biol.* **34:** 52–60.
29. Murphy, A. J., M. Akhtari, S. Tolani, T. Pagler, N. Bijl, C. L. Kuo, M. Wang, M. Sanson, S. Abramowicz, C. Welch, et al. 2011. ApoE regulates hematopoietic stem cell proliferation, monocytosis, and monocyte accumulation in atherosclerotic lesions in mice. *J. Clin. Invest.* **121:** 4138–4149.

30. Ellacott, K. L., G. J. Morton, S. C. Woods, P. Tso, and M. W. Schwartz. 2010. Assessment of feeding behavior in laboratory mice. *Cell Metab.* **12:** 10–17.

31. Kim, J. K., J. J. Fillmore, M. J. Sunshine, B. Albrecht, T. Higashimori, D. W. Kim, Z. X. Liu, T. J. Soos, G. W. Cline, W. R. O'Brien, et al. 2004. PKC-theta knockout mice are protected from fat-induced insulin resistance. *J. Clin. Invest.* **114:** 823–827.

32. Nagareddy, P. R., A. J. Murphy, R. A. Stirzaker, Y. Hu, S. Yu, R. G. Miller, B. Ramkhelawon, E. Distel, M. Westerterp, L. S. Huang, et al. 2013. Hyperglycemia promotes myelopoiesis and impairs the resolution of atherosclerosis. *Cell Metab.* **17:** 695–708.

33. Distel, E., T. J. Barrett, K. Chung, N. M. Girgis, S. Parathath, C. C. Essau, A. J. Murphy, K. J. Moore, and E. A. Fisher. 2014. miR33 inhibition overcomes deleterious effects of diabetes mellitus on atherosclerosis plaque regression in mice. *Circ. Res.* **115:** 759–769.

34. Potteaux, S., E. L. Gautier, S. B. Hutchison, N. van Rooijen, D. J. Rader, M. J. Thomas, M. G. Sorci-Thomas, and G. J. Randolph. 2011. Suppressed monocyte recruitment drives macrophage removal from atherosclerotic plaques of *Apoe-/-* mice during disease regression. *J. Clin. Invest.* **121:** 2025–2036.

35. Rahman, K., Y. Vengrenyuk, S. A. Ramsey, N. R. Vila, N. M. Girgis, J. Liu, V. Gusarova, J. Gromada, A. Weinstock, K. J. Moore, et al. 2017. Inflammatory Ly6Chi monocytes and their conversion to M2 macrophages drive atherosclerosis regression. *J. Clin. Invest.* **127:** 2904–2915.

36. Ke, J. Y., K. L. Kliewer, E. M. Hamad, R. M. Cole, K. A. Powell, R. R. Andridge, S. R. Straka, L. D. Yee, and M. A. Belury. 2015. The flavonoid, naringenin, decreases adipose tissue mass and attenuates ovariectomy-associated metabolic disturbances in mice. *Nutr. Metab. (Lond.).* **12:** 1.

37. Ke, J. Y., R. M. Cole, E. M. Hamad, Y. H. Hsiao, B. M. Cotten, K. A. Powell, and M. A. Belury. 2016. Citrus flavonoid, naringenin, increases locomotor activity and reduces diacylglycerol accumulation in skeletal muscle of obese ovariectomized mice. *Mol. Nutr. Food Res.* **60:** 313–324.

38. Tolani, S., T. A. Pagler, A. J. Murphy, A. E. Bochem, S. Abramowicz, C. Welch, P. R. Nagareddy, S. Holleran, G. K. Hovingh, J. A. Kuivenhoven, et al. 2013. Hypercholesterolemia and reduced HDL-C promote hematopoietic stem cell proliferation and monocytosis: studies in mice and FH children. *Atherosclerosis.* **229:** 79–85.

39. Nagareddy, P. R., M. Kraakman, S. L. Masters, R. A. Stirzaker, D. J. Gorman, R. W. Grant, D. Dragoljevic, E. S. Hong, A. Abdel-Latif, S. S. Smyth, et al. 2014. Adipose tissue macrophages promote myelopoiesis and monocytosis in obesity. *Cell Metab.* **19:** 821–835.

40. Allister, E. M., E. E. Mulvihill, P. H. Barrett, J. Y. Edwards, L. P. Carter, and M. W. Huff. 2008. Inhibition of apoB secretion from HepG2 cells by insulin is amplified by naringenin, independent of the insulin receptor. *J. Lipid Res.* **49:** 2218–2229.

41. Lee, J., J. Liu, X. Feng, M. A. Salazar Hernandez, P. Mucka, D. Ibi, J. W. Choi, and U. Ozcan. 2016. Withaferin A is a leptin sensitizer with strong antidiabetic properties in mice. *Nat. Med.* **22:** 1023–1032.

42. Liu, J., J. Lee, M. A. Salazar Hernandez, R. Mazitschek, and U. Ozcan. 2015. Treatment of obesity with Celastrol. *Cell.* **161:** 999–1011.

43. Ma, X., L. Xu, A. T. Alberobello, O. Gavrilova, A. Bagattin, M. Skarulis, J. Liu, T. Finkel, and E. Mueller. 2015. Celastrol protects against obesity and metabolic dysfunction through activation of a HSF1-PGC1α transcriptional axis. *Cell Metab.* **22:** 695–708.

44. Thaiss, C. A., S. Itav, D. Rothschild, M. Meijer, M. Levy, C. Moresi, L. Dohnalova, S. Braverman, S. Rozin, S. Malitsky, et al. 2016. Persistent microbiome alterations modulate the rate of post-dieting weight regain. *Nature.* **540:** 544–551.

45. He, B., K. Nohara, N. Park, Y. S. Park, B. Guillory, Z. Zhao, J. M. Garcia, N. Koike, C. C. Lee, J. S. Takahashi, et al. 2016. The small molecule nobiletin targets the molecular oscillator to enhance circadian rhythms and protect against metabolic syndrome. *Cell Metab.* **23:** 610–621.